

STUDY ON VIBRATIONAL RELAXATION DYNAMICS OF PHENOL-WATER COMPLEX BY PICOSECOND TIME-RESOLVED IR-UV PUMP-PROBE SPECTROSCOPY IN A SUPERSONIC MOLECULAR BEAM

Yasunori Miyazaki¹⁾, Yoshiya Inokuchi¹⁾, Takayuki Ebata^{1)*}, Milena Petković²⁾

¹⁾*Department of Chemistry, Graduate school of Science, Hiroshima University, Higashi-Hiroshima, 739-8526, Japan*

²⁾*Faculty of Physical Chemistry, University of Belgrade, Studentski Trg 12, 11 158 Belgrade, Serbia*

A comparative study of vibrational energy relaxation (VER) between the monohydrated complexes of phenol- d_0 and phenol- d_1 is investigated in a supersonic molecular beam. The direct time-resolved measurement of energy redistribution from the phenolic OH/OD stretching mode of the phenol- d_0 -H₂O/phenol- d_1 -D₂O is performed by picosecond IR-UV pump-probe spectroscopy. Two complexes follow the same relaxation process that begins with the intramolecular vibrational energy redistribution (**IVR**) and the intermolecular vibrational energy redistribution (*IVR*), which is followed by the vibrational predissociation (VP). The difference in the relaxation lifetimes between them is discussed by anharmonic force field and RRKM calculations. Anharmonic analysis implies that intra- (**IVR**) and intermolecular (*IVR*) relaxations occur in parallel in the complexes. The RRKM-predicted dissociation (VP) lifetimes show qualitative agreement with the observed results, suggesting that VP takes place after the statistical energy distribution in the complexes.

1. INTRODUCTION

Vibrational energy relaxation (VER) plays a crucial role in thermalizing excited vibrational energy of solute molecules in solution.¹⁻⁶ There are two pathways of energy relaxation from the excited vibrational mode. One is intramolecular vibrational energy redistribution (**IVR**) known as an energy dissipation process within internal vibrations of the solute molecule, and the other is vibrational cooling (VC) known as an energy-flow process to accessible vibrations of solvent molecules. A relaxation lifetime of VC depends on the solute-solvent interaction, e.g. van der Waals force (electrostatic force), dispersion force, and hydrogen bond.⁷ In particular, since the hydrogen-bonded system is important for understanding the reactivity of biological processes, the dynamics of the OH bond has been the subject of ongoing research. The hydrogen-bonded OH bond is characterized by several spectroscopic features. First is a large spectral red-shift of the OH stretching vibration, which is interpreted by the weakening of the OH bond due to a partial occupation of the σ^* level from the lone pair of the hydrogen acceptor. Second is a spectral broadening that is attributed to the short lifetime caused by VER and the overlapped OH stretching bands of as many hydrogen-bonded configurations as possible in solution. In consequence, surrounding solvent molecules mask the intrinsic vibrational mode couplings and detailed mechanism of VER. For this reason, a study of an isolated complex in gas phase is essential to assess a vibrational dynamics.

The development of various laser-based electronic and vibrational spectroscopic methods under the supersonic-jet experiment has been successful to shed light on the structural and vibrational analysis of various complexes of aromatic molecules.⁸⁻¹¹ Among them, hydrogen-bonded phenol complex has been extensively studied both structurally¹²⁻³⁰ and dynamically³¹⁻³⁶ because of its characteristic sensitivity of the phenolic OH stretching vibration to the basicity of solvent molecule²³. A combination of the time-resolved method and the cooling by supersonic free jet expansion enables us to perform a real-time measurement of population change to seek the relaxation process. In our previous works, picosecond time-resolved IR-UV pump-probe spectroscopy was carried out to investigate the VER dynamics of the hydrogen-bonded complexes of phenol, such as site-dependent relaxation of the phenol dimer³⁷ and search for the energy dissipation pathway and its time scale of the phenol-solvent complexes. The former one clarified that the rate of energy relaxation from the proton-donating phenol is accelerated whereas the one from the proton-accepting phenol is almost unchanged. In the latter, we proposed the three-step energy relaxation model via two bath

states⁴⁰. The vibrational energy is first redistributed into the phenolic site (**IVR** with bath 1) and transferred to the whole body of the complex (*IVR* with bath 2), which results in the vibrational predissociation (VP). It is also found that a shortening of the **IVR** lifetime is strongly correlated with the hydrogen-bond strength and the VP tends to be non-RRKM where the dissociation takes places prior to the complete energy randomization.

In this paper, we present a precise picture of the vibrational relaxation dynamics of monohydrated phenol complex by comparing the influence of the excitation energy on the VER lifetime using deuterium substituted species. Figure 1 shows the energy level and VER scheme for (a) the hydrogen system ($C_6H_6OH-H_2O$, phenol- d_0-H_2O) and (b) the deuterium system ($C_6H_5OD-D_2O$, phenol- d_1-D_2O). The IR spectrum in the inset on the left indicates the phenolic OH stretching at 3525 cm^{-1} and the phenolic OD stretching at 2600 cm^{-1} . The real-time energy redistribution from the phenolic OH/OD vibrational mode is studied by using picosecond time-resolved IR-UV pump-probe spectroscopy. The difference of the obtained rate constants between the two complexes is discussed based on two theoretical approaches: anharmonic force field and Rice-Ramsperger-Kassel-Marcus (RRKM) calculations. They support our pump-probe experimental results and emphasize important mode-to-mode vibrational couplings that alter the dissociative rate constant of the hydrogen-bonded phenol-water complex where the dissociation takes place after the complete energy randomization.

Figure 1

2. Experiment

A. Molecular beam and picosecond time-resolved IR-UV pump-probe system

Internally cold gaseous phenol- d_0-H_2O (or phenol- d_1-D_2O) is produced by a supersonic free jet expansion of the phenol- d_0/H_2O (or phenol- d_1/D_2O) gas mixture seeded in He carrier gas at the total pressure of 3 bar through a pulsed nozzle. The jet is collimated by a skimmer, which is located at 30 mm downstream of the nozzle. In the case of phenol- d_1-D_2O , all tubes and a nozzle were washed with D_2O beforehand to maintain the isotopically pure condition. The complex in the molecular beam is irradiated by picosecond IR and UV laser pulses for measuring the VER process of the complexes. The IR laser pulse (with energy $50\text{ }\mu\text{J}$) pumps the phenolic OH (or OD) stretching mode of the phenol- d_0-H_2O (or phenol- d_1-D_2O). By controlling an optical delay line, a tunable picosecond UV laser pulse (with energy $50\text{ }\mu\text{J}$) is

irradiated to monitor the population change of the pumped level and intra- and intermolecularly energy redistributed levels of the complex by resonant two-photon ionization (R2PI) via the S_1 state. The ionized species is mass-analyzed by a 50 cm time-of-flight tube and detected by a channeltron as an ion signal. An ion signal integrated by a boxcar integrator was processed on a personal computer. For the transient R2PI spectrum, ion intensity is recorded as a function of UV frequency at the fixed delay time after IR excitation. For the time profile, the IR-UV pump-probe ion signals are recorded by managing the computer-controlled optical delay lines of the UV laser pulse at the fixed UV frequency. To determine the lifetime τ , the time evolution of the excited vibrational level and bath states is convoluted with IR and UV laser pulse as a Gaussian line shape of 12 ps (FWHM). The tunable picosecond UV and IR laser pulses are obtained by the mode-locked Nd:YAG picosecond laser pumped OPG/OPA laser systems. The third harmonic of the mode-locked Nd:YAG picosecond laser (Expra PL2143B) is divided into two to pump two OPG/OPA laser systems, one (Expra PG401/DFG) generates a tunable IR laser pulse by difference frequency generation (DFG) between the idler light of OPG/OPA and 1.064 μm fundamental, the other (Expra PG401SH) generates a tunable UV light by frequency doubling the OPG/OPA visible output. The spectral resolution of the IR and UV laser pulses are 5 cm^{-1} .

B. Sample preparation

Phenol- d_0 (>99.5 %) and D_2O (isotopic purity >99.7 %) were used without further purifications. Phenol- d_1 was synthesized by D_2O and phenol- d_0 and purified simultaneously by vacuum sublimation as follows. An adequate amount of phenol- d_0 was placed in an excess amount of D_2O in the sublimation apparatus. It was immersed in a mild hot water bath (approximately 40 °C) for 1 hour. After removal of water by a vacuum pump, phenol- d_1 was obtained as a white crystal on the cooled surface.

C. Calculations

Density functional theory was employed to calculate the most stable ground-state structure, vibrational frequencies, and rotational constants of phenol- d_0 , phenol- d_1 , H_2O , D_2O , phenol- d_0 - H_2O and phenol- d_1 - D_2O using the M05-2X functional with a 6-31++G(d,p) basis set on the Gaussian 09 program package⁴¹. The optimized structure of the complex has the C_s symmetry with a plane of the water molecule orthogonal to the aromatic plane. To correct for

anharmonicity, the calculated vibrational frequencies of phenol- d_0 -H₂O and phenol- d_1 -D₂O are scaled by 0.9432 and 0.9532 in comparison to the phenolic OH and OD stretching frequencies in the IR spectrum, respectively. The rotational constants of phenol- d_0 , phenol- d_1 , H₂O, and D₂O are in good agreements with the experimental values¹²⁻¹³. The cubic force field analysis was performed at the B3LYP/6-311++G(2df, 2p) level calculation⁴².

3. Results

A. phenol- d_1 -D₂O

Figure 2 shows the transient R2PI spectra of phenol- d_1 -D₂O complex recorded at several delay times after the IR laser excitation to the phenolic OD stretching mode. These spectra are depicted in the manner that the R2PI spectrum without the IR laser irradiation is subtracted. It is clear that the energy flow is observed in two domains. A sharp band at 33410 cm⁻¹, assigned to the OD₁⁰ transition, rapidly disappears within 50 ps. On the other hand, a broad continuum, assigned to the vibronic transitions from the bath state at the isoenergetic level of the phenolic OD stretching mode, starts to appear in the frequency region higher than 34500 cm⁻¹. Therefore, the energy introduced to the OD stretch is rapidly redistributed to the whole body of the complex via **IVR** and *IVR*. The unusual intensity drop at ~ 35000 cm⁻¹ region (marked by asterisks) is due to the weak UV output. No ion signal is detected after the delay time of 280 ps since the complex dissociates by breaking the hydrogen bond.

Figure 2

The time profile of the pump-probe ion signals is analyzed by adopting a previously proposed three-step relaxation model for describing the VER of the phenol-solvent complexes³⁸⁻⁴⁰. In short, the OX (X=H or D) stretching energy is first redistributed into bath state 1 with a lifetime τ_1 and the energy is further transferred to bath state 2 with a lifetime τ_2 , followed by the dissociation of the complex with a lifetime τ_3 . Here, bath state 1 is built by dense vibrational levels consisting of mostly the intramolecular modes of the phenolic site and bath state 2 mostly consists of the intermolecular modes of the complex. The transition intensities from bath state 1 and bath state 2 depend on Franck-Condon factors from the energy-transferred levels. The time evolution of each bath state is expressed in the following equations,⁴⁵

$$I_{\text{ox}}(t) = C_0 \exp\left(-\frac{t}{\tau_1}\right) \quad (1)$$

$$I_{\text{bath1}}(t) = C_{b1} \left[-\exp\left(-\frac{t}{\tau_1}\right) + \exp\left(-\frac{t}{\tau_2}\right) \right] \quad (2)$$

$$I_{\text{bath2}}(t) = C_{b2} \left[\left(\frac{1}{\tau_2} - \frac{1}{\tau_3}\right) \exp\left(-\frac{t}{\tau_1}\right) + \left(\frac{1}{\tau_3} - \frac{1}{\tau_1}\right) \exp\left(-\frac{t}{\tau_2}\right) + \left(\frac{1}{\tau_1} - \frac{1}{\tau_2}\right) \exp\left(-\frac{t}{\tau_3}\right) \right] \quad (3)$$

Based on this model, a least squares fitting method is used to find the best-fit lifetimes and coefficients that reproduce the observed time profiles (⊙) in Figure 3. The population change at the phenolic OD stretch level is monitored by the OD₁⁰ transition at 33410 cm⁻¹. As seen in Figure 3a, the **IVR** lifetime (τ₁) is determined by fitting a single exponential decay curve, which yields 12 ps. Since the broad continuum consists of the transitions of bath states 1 and 2, the time evolution measured at the broad continuum is expressed by the sum of I_{bath1}(t) and I_{bath2}(t). The fitting of the time evolutions at three different probe UV frequencies seen in figure 3b), c), and d) yields the *IVR* lifetime (τ₂) of 24 ps and the VP lifetime (τ₃) of 100 ps. The ratio of the transition intensities of bath state 1 (C_{b1}) and bath state 2 (C_{b2}) is different at each probe UV frequency as expected. In other words, there are larger *IVR* contributions at higher UV frequency because the electronic transitions of low frequency intermolecular vibrational modes (bath 2) are Franck-Condon allowed near the S₀-S₁ band origin (36000 cm⁻¹)³⁸.

Figure 3

B. phenol-*d*₀-H₂O

The same IR-UV pump-probe experiment has been performed for the phenol-*d*₀-H₂O, as shown in figure 4. The decay time profile of the IR excited OH stretching level was not measured as our laser system did not generate a monitoring UV light at 32476 cm⁻¹ that corresponds to the OH₁⁰ transition. Thus, we used the **IVR** lifetime (τ₁) estimated from the bandwidth of the OH band in the IR spectrum by Doi and Mikami⁴³, which is 4 ps. The analysis of the time evolution at the broad continuum seen in figure 4a), b), and c) yields the *IVR* lifetime (τ₂) of 6 ps and the VP lifetime (τ₃) of 40 ps. As with the deuterium system, the ratio of the transition intensities of bath 1 and bath 2 changes in accordance with the probe UV frequency.

Figure 4

4. Discussion

In order to evaluate the relaxation process of phenol-water complex, we adapted “three-step relaxation model involving **IVR** and vibrational predissociation.” It was first proposed by Ebata and coworkers for describing the VER of the hydrogen-bonded phenol complex with solvent molecules³⁸⁻⁴⁰ and its validity was recently confirmed from the VER of benzene dimer and trimer⁴⁴. The lifetimes of phenol-water complex utilized by this model are summarized in Table 1. In this section, we discuss the VER mechanism and rate constants by comparing the experimental results with those of the anharmonic forced field calculation and RRKM calculation.

Table 1

A. Anharmonic Force Field Calculation Study

We first discuss the relaxation pathways from the phenolic OH and OD stretching modes, ν_{OH} and ν_{OD} , respectively, in terms of anharmonic force field study⁴¹. This treatment was first reported by Petković⁴², providing the line-up candidates of the combination modes that couple to the ν_{OH} of phenol and its hydrogen-bonded complexes. The potential function of vibrations is expanded by Taylor series around the global minimum as

$$V(Q) = V|_{Q=0} + \frac{1}{2!} \sum_i \frac{\partial^2 V}{\partial Q_i^2} \Big|_{Q=0} Q_i^2 + \frac{1}{3!} \sum_{i,j,k} \frac{\partial^3 V}{\partial Q_i \partial Q_j \partial Q_k} \Big|_{Q=0} Q_i Q_j Q_k + \frac{1}{4!} \sum_{i,j,k,l} \frac{\partial^4 V}{\partial Q_i \partial Q_j \partial Q_k \partial Q_l} \Big|_{Q=0} Q_i Q_j Q_k Q_l + \dots \quad (4)$$

Table 2 lists the overtone and combination levels which couple with $\nu_{\text{OH/OD}}$ via the cubic anharmonic term and the coupling constants ($K_{ij\nu_{\text{OH}}}$) larger than 300 cm^{-1} . It should be noted that the energy gap is not satisfied to be isonergetic at this stage and higher-order coupling is required to hold the energy conservation involving the vibrational quanta between modes, but these combinations are still possible candidates for initiating the energy transfer from $\nu_{\text{OH/OD}}$. First, two systems (phenol- d_0 -H₂O and phenol- d_1 -D₂O) have almost equal number of available coupling levels that promote **IVR** and **IVR** through the intramolecular modes and intermolecular modes. Especially, in both cases, the strong coupling of $\nu_{\text{OH/OD}}$ with the out-

of-pane torsion $\tau_{\text{OH/OD}}$ leads **IVR** while the one with the intermolecular modes, i.e. torsional motion of water molecule, leads *IVR*. These outcomes imply that **IVR** occurs in parallel with *IVR* in the VER. Second, phenol- d_0 -H₂O has twice as many intra- and intermolecular coupling levels as phenol- d_1 -D₂O. In addition, we see that the phenolic CH vibrations are also anharmonically coupled with ν_{OH} , which is in good agreement with our previous study that the vibrations involving the CH groups are also the possible candidates to promote **IVR** of phenol- d_0 -H₂O.⁴⁵ Therefore, the hydrogen system would be more likely to dissipate energy than the deuterated system, resulting in the shorter lifetime of **IVR** and *IVR*, as is observed.

Table 2

B. RRKM theory estimation

After the rapid energy redistribution, the complexes dissociate by vibrational predissociation (VP). Here, we discuss whether the dissociation can be treated by statistical theory calculation to describe the observed VP rate constants and the difference of the constants between the two complexes⁴⁶⁻⁵¹. According to the RRKM theory, a dissociation rate constant $k(E)$ is given by

$$k(E) = \frac{1}{h} \frac{W(E - E_D)}{\rho(E)}. \quad (5)$$

where $\rho(E)$ is the vibrational state densities at the phenolic OH/OD stretching energy E of the complex, E_D is the hydrogen-bond dissociation energy, and $W(E - E_D)$ is the total number of quantum states of the complex at the transition state with an excess energy of $E - E_D$. Figure 5 is the schematic potential energy diagram of the two phenol-water complexes along the hydrogen-bond distance. The vibrational state density $\rho(E)$ is estimated by direct counting method using harmonic oscillator from the energy optimized structure of the complexes at M05-2X/6-31++G(d,p) level. Since the complexes has a C_s symmetry, only the A' vibrational modes as that of the OH/OD stretching mode are taken into account. Courty et al. measured the accurate dissociation energy E_D to be $1958 \pm 38 \text{ cm}^{-1}$ for phenol- d_0 -H₂O⁵². Assuming that the two systems possess the equal hydrogen-bond strength, we set E_D 2000 cm^{-1} that gives their excess energies of 1525 cm^{-1} and 600 cm^{-1} for phenol- d_0 -H₂O and phenol- d_1 -D₂O, respectively.

Figure 5

The prediction of the transition state is very difficult since the dissociation is thought to occur without a barrier. Instead, we assumed that the intermolecular vibrational modes at the transition state can be replaced by the rotational motion of the fragments with a restriction of the conservation of angular momentum between the complex and the fragments. Then, $W(E-E_D)$ is expressed by

$$W(E-E_D) = \sum N_v(E_v) N_R(E_R, J). \quad (6)$$

Here, $N_v(E_v)$ is the number of the vibrational states at the energy E_v , and $N_R(E_R, J)$ is the number of the rotational states at the energy $E_R = E - E_D - E_v$ with the total angular momentum of J . Though both the complex and the fragment molecules must have J and K structures, we approximated them as diatomic rigid molecules with the rotational axis of the largest moment of inertia in each species. That is,

$$E_R = E - E_D - E_v = B_{\text{ph}} J_{\text{ph}}(J_{\text{ph}}+1) + B_{\text{w}} J_{\text{w}}(J_{\text{w}}+1). \quad (7)$$

Here, B_{ph} and B_{w} are the rotational constants of phenol and water, respectively, and J_{ph} and J_{w} are the quantum numbers of the angular momentum of phenol and water, respectively. The temperature of the complexes in a molecular beam is assumed to be 10 K, giving the prominent distribution of $J = 0 - 40$ in both complexes. Table 3 lists the calculated dissociation lifetime (τ_{RRKM}) for the two complexes. Though the calculated values are roughly 2.5 -3 times slower than those of the observed ones, we consider the agreement is reasonable based on the simplicity of the model. In addition, the ratio of the observed VP lifetime (τ_3) between phenol- d_0 -H₂O and phenol- d_1 -D₂O is also reproduced by the RRKM calculation. Thus, we conclude the hydrogen-bond dissociation occurs after the complete energy randomization in both complexes.

Table 3

5. Conclusion

In summary, we applied picosecond time-resolved IR-UV pump-probe spectroscopy to investigate vibrational dynamics of the phenol-water complex starting from the phenolic OH/OD stretching vibration of phenol- d_0 -H₂O and phenol- d_1 -D₂O. The transient R2PI spectra indicate the evident energy flow from the phenolic OH/OD stretching mode to intra-

and intermolecular vibrational modes in the complex. To pursue the energy redistribution route in the complex, time profiles of IR-UV pump-probe signals are measured at several UV frequencies and they are analyzed by the three-step relaxation model. The anharmonic force field calculation for searching energy-flow pathway via the vibrational mode couplings showed that the number of coupled levels with the OH stretch is greater than the one with the OD stretch, which support our experimental results. The lifetime of the H-bond dissociation of the complexes can be treated by the RRKM theory calculation, suggesting a statistical distribution before breaking the H-bond. Also the model describes the difference of the VP lifetimes between the two complexes. These two theoretical model can well describe internal events of energy redistribution and randomization of VER in the complex starting from the OX(X=H and D) stretching vibration.

Acknowledgments

This work is supported by MEXT for the Scientific Research on Priority Area “Molecular Science for Supra Functional Systems” (No. 477).

References

- ¹A. J. Lock, S. Woutersen, and H. J. Bakker, *J. Phys. Chem. A* **105**, 1238 (2001).
- ²A. Pakoulev, Z. Wang, Y. Pang, and D. D. Dlott, *Chem. Phys. Lett.* **380**, 404 (2003).
- ³S. L. Tesar, V. M. Kasyanenko, I. V. Rubtsov, G. I. Rubtsov, and A. L. Burin, *J. Phys. Chem. A* **117**, 315 (2013).
- ⁴M. J. Cox and F. F. Crim, *J. Phys. Chem. A* **109**, 11673 (2005).
- ⁵K. A. Briney, L. Herman, D. S. Boucher, A. D. Dunkelberger, and F. F. Crim, *J. Phys. Chem. A* **114**, 9788 (2010).
- ⁶M. Sakai and M. Fujii, *Chem. Phys. Lett.* **396**, 298 (2004).
- ⁷J. C. Owrutsky, D. Raftery, and R. M. Hochstrasser, *Annu. Rev. Phys. Chem.* **45**, 519 (1994).

- ⁸ M. Ito, *J. Mol. Struct.* **177**, 173 (1988).
- ⁹ A. Fujii, S. Morita, M. Miyazaki, T. Ebata, N. Mikami, *J. Phys. Chem. A* **108**, 2652 (2004).
- ¹⁰ T. Nakanaga, N. K. Piracha, and F. Ito, *J. Phys. Chem. A* **105**, 4211 (2001).
- ¹¹ P. K. Chowdhury, *J. Phys. Chem. A* **107**, 5692 (2003).
- ¹² G. Berden, W. L. Meerts, M. Schmitt, and K. Kleinermanns, *J. Chem. Phys.* **104**, 972 (1996).
- ¹³ R. M. Helm and H. J. Neusser, *Chem. Phys.* **239**, 33 (1998).
- ¹⁴ R. J. Stanley and A. W. Castleman, Jr, *J. Chem. Phys.* **94**, 7744 (1991).
- ¹⁵ R. J. Stanley and A. W. Castleman, Jr, *J. Chem. Phys.* **98**, 796 (1993).
- ¹⁶ T. Watanabe, T. Ebata, S. Tanabe, and N. Mikami, *J. Chem. Phys.* **105**, 408 (1996).
- ¹⁷ T. Ebata, K. Nagao, and N. Mikami, *J. Chem. Phys.* **231**, 199 (1998).
- ¹⁸ T. Ebata, N. Mizuochi, T. Watanabe, and N. Mikami, *J. Phys. Chem.* **100**, 546 (1996).
- ¹⁹ M. Schmitt, Ch. Jacoby, and K. Kleinermanns, *J. Chem. Phys.* **108**, 4486 (1998).
- ²⁰ S. Tanabe, T. Ebata, M. Fujii, and N. Mikami, *Chem. Phys. Lett.* **215**, 347 (1993).
- ²¹ M. Schutz, T. Burgi, and S. Leutwyler, *J. Chem. Phys.* **98**, 3763 (1993).
- ²² T. Ebata, T. Watanabe, and N. Mikami, *J. Phys. Chem.* **99**, 5761 (1995).
- ²³ A. Iwasaki, A. Fujii, T. Watanabe, T. Ebata, and N. Mikami, *J. Phys. Chem.* **100**, 16053 (1996).
- ²⁴ A. Schiefke, C. Deusen, C. Jacoby, M. Gerhards, and M. Schmitt, *J. Chem. Phys.* **102**, 9197 (1995).
- ²⁵ G. V. Hartland, B. F. Henson, V. A. Venturo, and P. M. Felker, *J. Phys. Chem.* **96**, 1164 (1992).
- ²⁶ Ch. Plutzer, Ch. Jacoby, and M. Schmitt, *J. Phys. Chem. A* **106**, 3998 (2002).
- ²⁷ J. Kupper, A. Westphal, and M. Schmitt, *Chem. Phys.* **263**, 41 (2001).
- ²⁸ A. Fujii, T. Ebata, and N. Mikami, *J. Phys. Chem. A* **106**, 8554 (2002).

- ²⁹ A. Fujii, T. Ebata, and N. Mikami, *J. Phys. Chem. A* **106**, 10124 (2002).
- ³⁰ D. Spangenberg, P. Imhof, W. Roth, Ch. Janzen, and K. Kleinermanns, *J. Phys. Chem. A* **103**, 5918 (1999).
- ³¹ Y. L. Rezus, D. Madsen, and H. J. Bakker, *J. Chem. Phys.* **121**, 10599 (2004).
- ³² T. Ebata, A. Iwasaki, and N. Mikami, *J. Phys. Chem. A* **104**, 7974 (2000).
- ³³ J. L. Knee, L. R. Khundkar, and A. H. Zewail, *J. Chem. Phys.* **87**, 115 (1987).
- ³⁴ G. Gregoire, C. Dedonder-Lardeux, C. Jouvet, S. Martrenchard, A. Peremans, and D. Solgadi, *J. Phys. Chem. A* **104**, 9087 (2000).
- ³⁵ R. J. Lipert and S. D. Colson, *J. Phys. Chem.* **93**, 135 (1989).
- ³⁶ A. L. Sobolewski and W. Domcke, *J. Phys. Chem. A* **105**, 9275 (2001).
- ³⁷ T. Ebata, M. Kayano, S. Sato, and N. Mikami, *J. Phys. Chem. A* **105**, 8623 (2001).
- ³⁸ M. Kayano, T. Ebata, Y. Yamada, and N. Mikami, *J. Chem. Phys.* **120**, 7410 (2004).
- ³⁹ Y. Yamada, M. Kayano, N. Mikami, and T. Ebata, *J. Phys. Chem. A* **110**, 6250 (2006).
- ⁴⁰ Y. Yamada, Y. Katsumoto, and T. Ebata, *Phys. Chem. Chem. Phys.* **9**, 1170 (2007).
- ⁴¹ M. J. Frisch, G. W. Trucks, H. B. Schlegel, G. E. Scuseria, M. A. Robb, J. R. Cheeseman, G. Scalmani, V. Barone, B. Mennucci, G. A. Petersson *et al.*, Gaussian 09, revision A.02; Gaussian, Inc.: Wallingford, CT, (2009).
- ⁴² M. Petković, *J. Phys. Chem. A* **116**, 364 (2012).
- ⁴³ A. Doi and N. Mikami, *J. Chem. Phys.* **129**, 154308 (2008).
- ⁴⁴ R. Kusaka and T. Ebata, *J. Phys. Chem. A* **136**, 044304 (2012).
- ⁴⁵ Y. Yamada, T. Ebata, M. Kayano, N. Mikami, *J. Chem. Phys.* **120**, 7400 (2004).
- ⁴⁶ D. J. Nesbitt and R. W. Field, *J. Phys. Chem.* **100**, 12735 (1996).
- ⁴⁷ F. F. Crim, *J. Phys. Chem.* **100**, 12725 (1996).
- ⁴⁸ R. A. Marcus, W. L. Hase, and K. N. Swamy, *J. Phys. Chem.* **88**, 6717 (1984).
- ⁴⁹ L. R. Khundkar, R. A. Marcus, and A. H. Zewail, *J. Phys. Chem.* **87**, 2473 (1983).
- ⁵⁰ J. L. Knee, L. R. Khundkar, and A. H. Zewail, *J. Phys. Chem.* **89**, 4659 (1985).

⁵¹ D. F. Kelly and E. R. Bernstein, *J. Phys. Chem.* **90**, 5164 (1986).

⁵² A. Courty, M. Mons, I. Dimicoli, F. Piuzzi, V. Brenner, and P. Millie, *J. Phys. Chem. A* **102**, 4890 (1998).

TABLE 1. Fitted parameters from the pump-probe ion signals of each phenol-water complex.

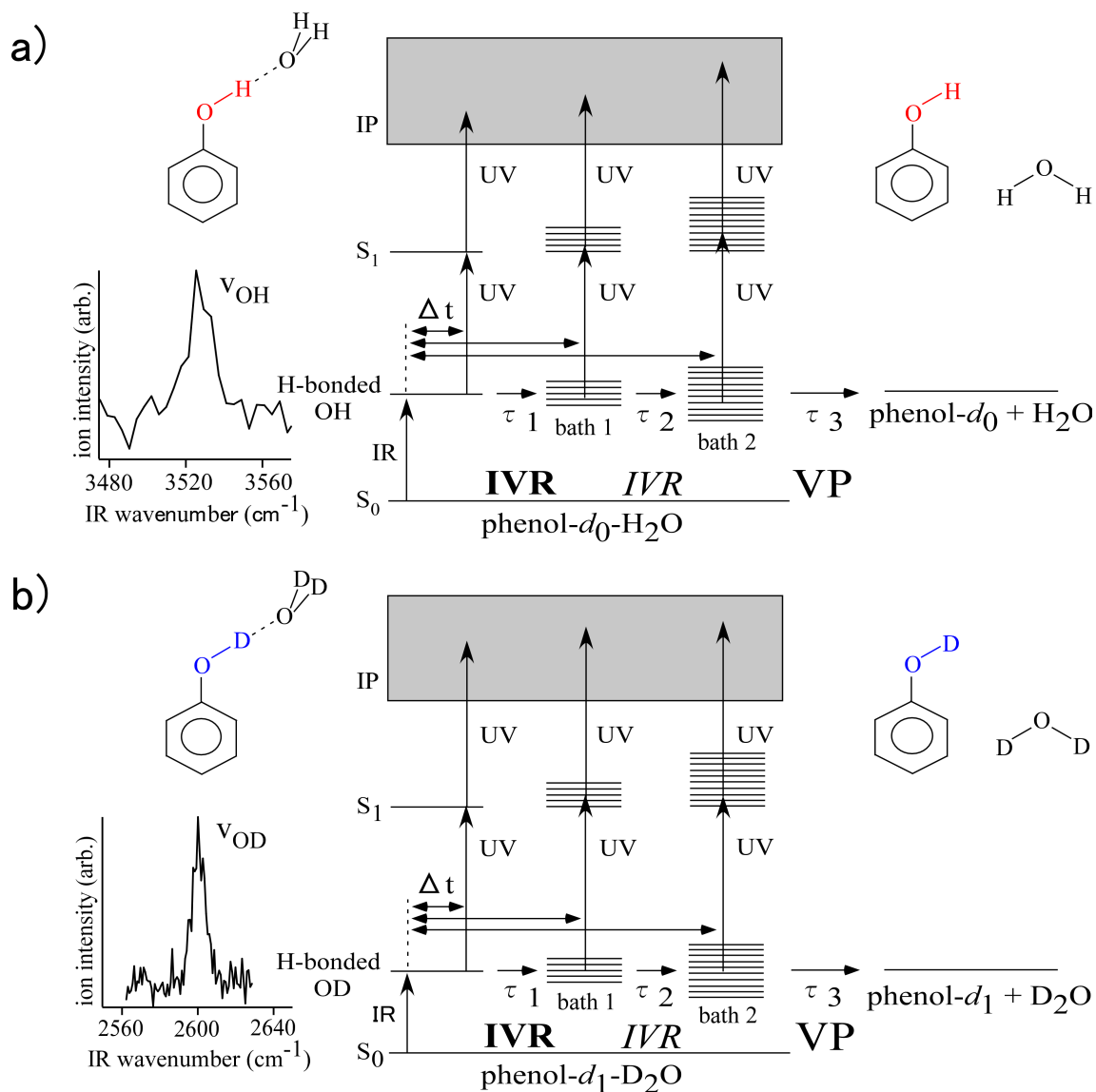
complex	stretching mode	frequency (cm^{-1})	excess energy (cm^{-1})	IVR τ_1 (ps)	<i>IVR</i> τ_2 (ps)	VP τ_3 (ps)
phenol- d_0 -H ₂ O	ν_{OH}	3525	1525	4	6	40
phenol- d_1 -D ₂ O	ν_{OD}	2600	600	12	24	100

TABLE 2. Cubic anharmonic force constant $K_{ij\nu_{\text{OH}}}$ (absolute values in cm^{-1}) involving the OH/OD stretching mode in phenol- d_0 -H₂O/phenol- d_1 -D₂O larger than 300 cm^{-1} . Each superscript on the vibrational mode is numbered in the order from the lowest vibrational frequency of the calculation.

phenol- d_0 -H ₂ O				phenol- d_1 -D ₂ O			
mode i	mode j	$K_{ij\nu_{\text{OH}}}$	promoting	mode i	mode j	$K_{ij\nu_{\text{OD}}}$	promoting
γ_{OH}	γ_{OH}	1514	IVR	γ_{OD}	γ_{OD}	1026	IVR
γ_{OH}	$\tau_{\text{H}_2\text{O}}^7$	676	IVR & <i>IVR</i>	γ_{OD}	$\tau_{\text{D}_2\text{O}}^5$	542	IVR & <i>IVR</i>
$\tau_{\text{H}_2\text{O}}^3$	$\tau_{\text{H}_2\text{O}}^3$	529	<i>IVR</i>	$\tau_{\text{D}_2\text{O}}^5$	$\tau_{\text{D}_2\text{O}}^5$	523	<i>IVR</i>
γ_{OH}	$\tau_{\text{H}_2\text{O}}^5$	497	IVR & <i>IVR</i>	$\tau_{\text{D}_2\text{O}}^3$	$\tau_{\text{D}_2\text{O}}^3$	445	<i>IVR</i>
$\tau_{\text{H}_2\text{O}}^7$	$\tau_{\text{H}_2\text{O}}^7$	493	<i>IVR</i>	δ_{OD}^{20}	δ_{OD}^{20}	415	IVR
δ_{OH}^{26}	δ_{OH}^{26}	406	IVR				
$\tau_{\text{H}_2\text{O}}^7$	$\tau_{\text{H}_2\text{O}}^5$	400	<i>IVR</i>				
γ_{CH}^{15}	γ_{OH}	347	IVR				
$\tau_{\text{H}_2\text{O}}^5$	$\tau_{\text{H}_2\text{O}}^5$	321	<i>IVR</i>				
δ_{CH}^{29}	δ_{OH}^{26}	309	IVR				

TABLE 3. Calculated vibrational state density $\rho(E)$ and total number of rotational and vibrational states of the fragments W, and predicted dissociation lifetime τ_{RRKM} .

complex	$\rho(E) \times 10^5$ (cm)	W(E-E _D) $\times 10^5$	τ_{RRKM} (ps)	expt τ_3 (ps)
phenol- d_0 -H ₂ O	1.85	14.8	100	40
phenol- d_1 -D ₂ O	0.786	1.91	330	100



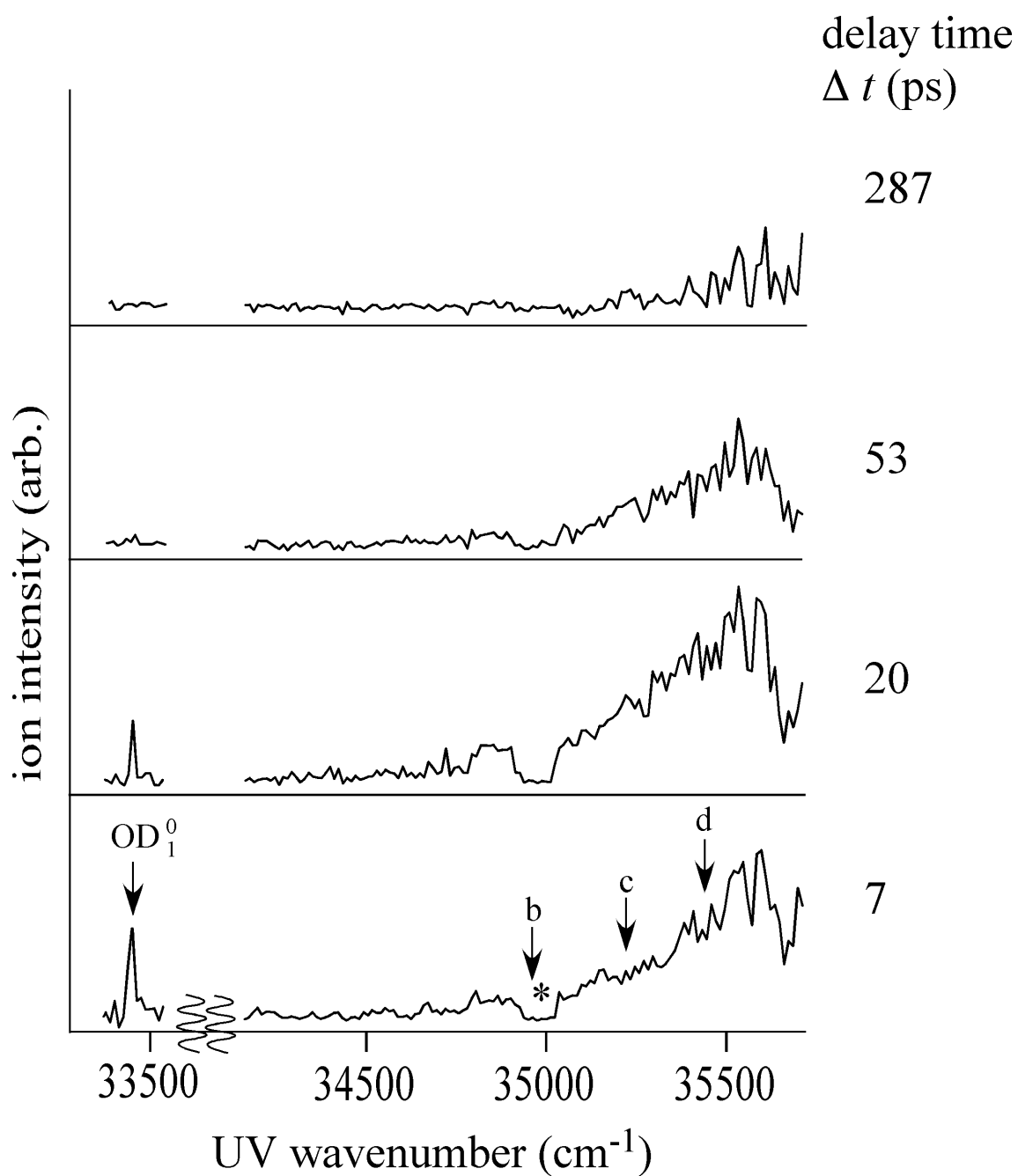


FIG. 2. Transient R2PI spectra of phenol- d_1 -D₂O measured at the delay times of 7 ps, 20 ps, 53 ps, and 287 ps after the IR excitation of the phenolic OD stretching mode. The region between 33500 cm^{-1} and 34000 cm^{-1} is omitted because no prominent signal appears there. A lack of the ion intensity between 34800 and 35100 cm^{-1} is caused by unadjusted SHG crystal angle in the laser system. The timed profiles were observed at the positions marked by arrows.

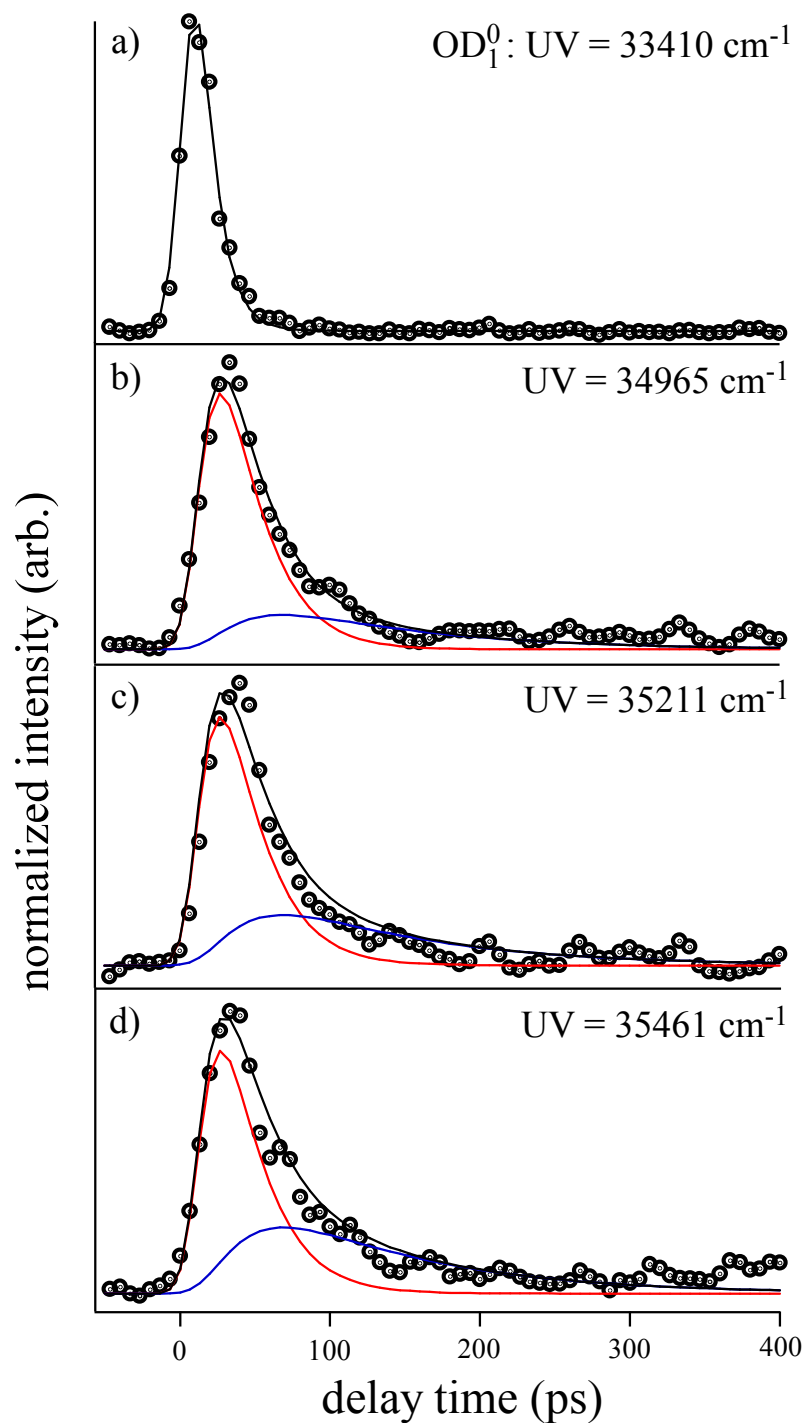


FIG. 3. Time evolution of phenol- d_1 -D₂O at four different probe UV frequencies: (a) OD_1^0 band, and (b)-(d) bath states. The dotted circles are the experimental pump-probe ion signals. The red and blue lines represent the population change at bath 1 and bath 2, respectively. See text.

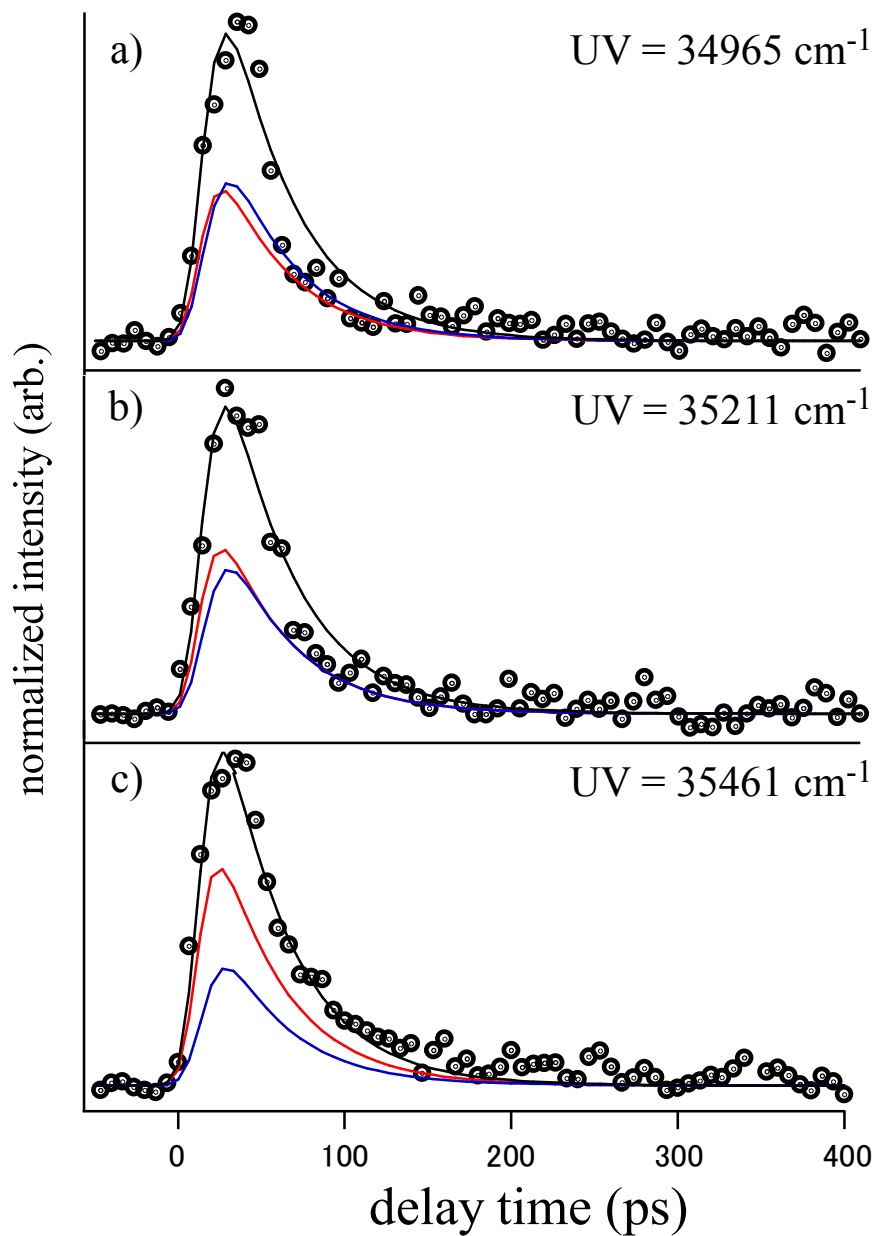


FIG. 4. Time evolution of phenol- d_0 -H₂O at three different probe UV frequencies that correspond to bath states. The dotted circles are the experimental pump-probe ion signals. The red and blue lines represent the population change at bath 1 and bath 2, respectively. See text.

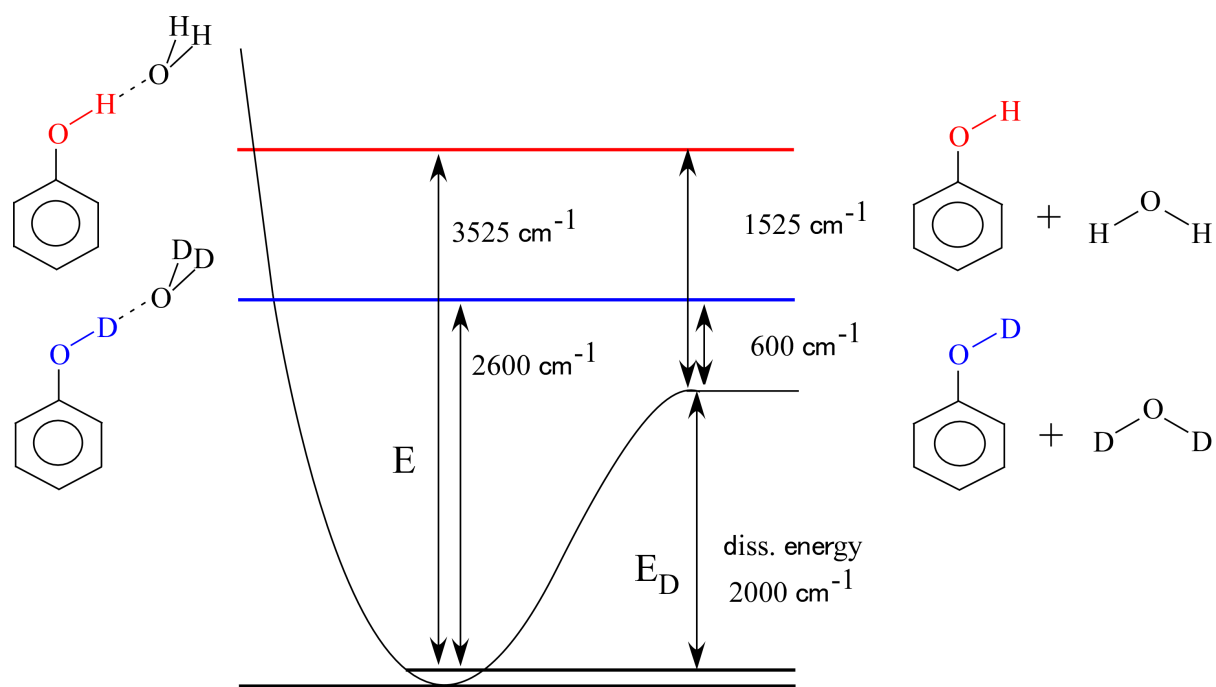


FIG. 5. Schematic potential energy diagram of the phenol- d_0 - H_2O and phenol- d_1 - D_2O complexes along the hydrogen-bond coordinate.

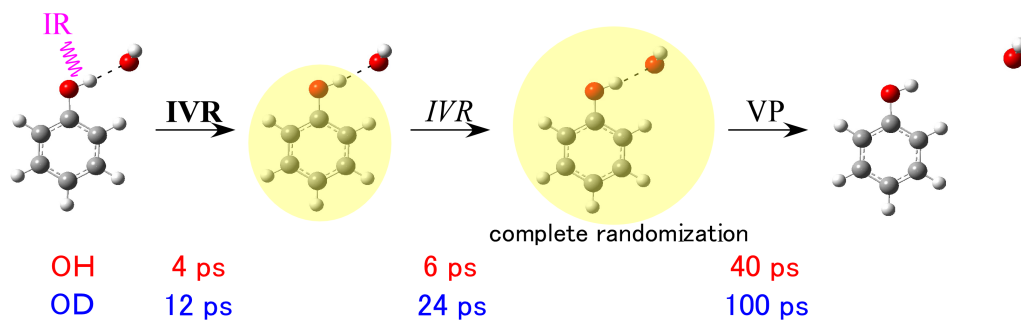


Table of Graphics